J. Fluid Mech. (1979), *vol.* 95, *part* 3, *pp.* 415–429
Printed in Great Britain

Low-Reynolds-number motion of particles with two or three perpendicular planes of symmetry

By J. B. HARRIS†, M. NAWAZ AND J. F. T. PITTMAN

Department of Chemical Engineering, University College of Swansea, Singleton Park, Swansea SA2 8PP, U.K.

(Received 28 September 1978 and in revised form 18 May 1979)

For a particle with two or three perpendicular planes of symmetry rotating at low Reynolds number in a Couette flow field, there are three orbits in which the motion is simply periodic. The three scalars B_i involved in Bretherton's shape tensor are found experimentally from periods of rotation in these orbits. Experiments on right parallelepipeds, ranging from thin platelets through cubes to rectangular section rods, are described. Each of the B_i is found to depend on the aspect ratio of one of the particle cross-sections, with only slight influence from its third dimension. Results are expressed in terms of a relationship between this aspect ratio and that of an equivalent ellipse, incorporating a weak function of the third particle dimension. The equations of motion governing a general doubly periodic motion, and incorporating experimental B_i values, are integrated numerically and compared satisfactorily with experimental observations.

1. Introduction

Our starting point is Bretherton's (1962) equation for the angular velocity ω_i of a neutrally buoyant, rigid particle suspended in a linear velocity field at low Reynolds number,

$$\omega_i = \zeta_i + \tfrac{1}{2}B_{ijk}\Delta_{jk}, \tag{1}$$

where ζ_i is half the vorticity and Δ_{jk} the rate of deformation tensor. Conditions for its applicability are discussed in Brenner (1962, 1964), but in practice an important limitation on its use is our knowledge of the component values of the shape tensor B_{ijk} corresponding to various particles.

For a particle with two or three mutually perpendicular planes of symmetry there are six non-zero components (Bretherton 1962; Brenner 1964)

$$B_{123} = B_{132} = B_1, \quad B_{213} = B_{231} = B_2 \quad \text{and} \quad B_{312} = B_{321} = B_3. \tag{2}$$

The classical result derived by Jeffery (1922) for an ellipsoid with semi-axes a_1, a_2, a_3 gives

$$B_1 = (r_1^2-1)/(r_1^2+1), \tag{3a}$$

$$B_2 = -(r_1^2-1)/(r_2^2+1) \tag{3b}$$

and

$$B_3 = (r_3^2-1)/(r_3^2+1), \tag{3c}$$

where $r_1 = a_2/a_3$, $r_2 = a_1/a_3$ and $r_3 = a_1/a_2$.

† Present address: Unilever Research, Colworth, Bedfordshire.

0022–1120/79/4359–8080 $02.00

In more recent years there has been considerable progress in the analytical treatment of other particle shapes, but without exception these have been bodies of revolution. Youngren & Acrivos (1975) have presented a powerful numerical method for Stokes flow past a particle of arbitrary shape, and applied it to spheroids and cylinders. We shall not review the theoretical work, but only note that no results are yet available for platelets, cubes and similar sharp-edged, crystal-like particles, which are of considerable interest in suspension rheology. We are concerned here with the experimental determination of the components of B_{ijk} for these, and more generally for any particles with two or three mutually perpendicular planes of symmetry.

Experimental work on sharp-edged bodies of revolution, namely disks and cylinders (Goldsmith & Mason 1967; Harris & Pittman 1975) is available. The single scalar B involved in B_{ijk} in this case has been expressed in terms of an equivalent axis ratio p of an oblate or prolate spheroid

$$B = \frac{p^2 - 1}{p^2 + 1}. \tag{4}$$

Gierszewski & Chaffey (1978) recently proposed the experimental determination of B_1, B_2, B_3 for particles with two perpendicular symmetry planes. They suggest simultaneous observation along the $O1$ and $O2$ directions of a particle suspended in the simple shear

$$v_3 = \gamma x_2 \tag{5}$$

and measurement of the instantaneous values of the three Euler angles describing the particle orientation and their time derivatives. These, together with γ, would be substituted into the equations of motion which, being linear in B_1, B_2, B_3, could readily be solved for these quantities. They present the equations of motion, and illustrate the form of some orbits with results obtained by numerical integration.

Very recently, Hinch & Leal (1979) have analysed the motion of a non-axisymmetric ellipsoid in the simple shear field (5) and demonstrated the ordered structure underlying the very complicated orbits. The motion is shown to be doubly periodic, with 'a relatively rapid rotation which corresponds to the motion of axisymmetric particles around Jeffery orbits, and a slower drift which would be described as a periodic change in the orbit if the particle were axisymmetric'. They also investigated the stability of the three planar orbits obtained by aligning each of the ellipsoid axes in turn parallel to the vorticity. An important conclusion of their paper is that relatively small departures from axisymmetry result in profound changes in particle motion. Although the work refers specifically to ellipsoids, its conclusions on the structure and stability of orbits apply qualitatively to a wider class of particles with 2 or 3 perpendicular symmetry planes.

In the present paper we describe an experimental determination for B_1, B_2, B_3, which is somewhat simpler than that suggested by Gierszewski & Chaffey (1978). It involves observations along only the $O2$ direction and measurement of periods of rotation, which should be easier to obtain accurately than instantaneous rotation rates. We present results for particles in the shape of right parallelepipeds. The method is applicable to all particles with two or three perpendicular symmetry planes, and the resulting values for B_{ijk} allow prediction of the rotation of an isolated particle in any locally linear velocity field. While this falls far short of a complete solution to the Stokes flow problem it can have important uses when a suspension is sufficiently

dilute for the behaviour of an assembly of particles to be deduced from knowledge of single particle motion.

In a non-flocculating suspension, particle rotation and the resulting distribution of orientations will influence the bulk properties. Among these the most important is probably the deviatoric stress increment due to the suspended particles, but also included are transport properties and light scattering. The orientation of particles included in filled and reinforced plastics is usually determined by flow of a suspension prior to solidification, and this orientation has important effects upon the mechanical properties of the solid. (It should be mentioned, though, that in this case the suspending medium is generally non-Newtonian.)

In the field of flocculating suspensions interest has recently turned towards the role of hydrodynamic forces in influencing colloidal stability. For all particles other than spheres the question of relative orientation becomes important. One needs, as an initial condition for this very difficult problem of particle interaction, information on probable orientations as particles approach each other. Knowledge of single particle motion provides the starting point in determining this for dilute suspensions, in the absence of Brownian motion.

2. Equations of motion

The quantities ζ_i and Δ_{ij} in (1) are referred to Cartesian axes $O\,1'2'3'$ fixed in the particle. The orientation of these relative to axes $O\,1\,2\,3$ fixed in space is expressed in terms of the Euler angles (see figure 1) and the transformation matrix M_{ij} as quoted by Jeffery (1922), for example. Jeffery also gives the relationships between the angular velocities and the time derivatives of ϕ, θ, ψ:

$$\omega_1 = \dot{\phi}\cos\theta + \dot{\psi}, \tag{6a}$$

$$\omega_2 = \dot{\theta}\sin\psi - \dot{\phi}\sin\theta\cos\psi \tag{6b}$$

and

$$\omega_3 = \dot{\theta}\cos\psi + \dot{\phi}\sin\theta\sin\psi. \tag{6c}$$

For a particle with two or three perpendicular symmetry planes, we express from (1) the angular velocities in terms of vorticity and rate of deformation referred to $O\,1\,2\,3$ for the flow field of (5), then substitute in (6) and solve for the angle derivatives:†

$$\dot{\phi} = \tfrac{1}{2}\gamma + \tfrac{1}{2}\gamma[\tfrac{1}{2}(B_2+B_3)\cos\theta\sin 2\phi\sin 2\psi + \cos 2\phi(B_3\sin^2\psi - B_2\cos^2\psi)], \tag{7a}$$

$$\dot{\theta} = \tfrac{1}{2}\gamma[\tfrac{1}{2}\sin 2\theta\sin 2\phi(B_3\cos^2\psi - B_2\sin^2\psi) + \tfrac{1}{2}\sin\theta\cos 2\phi\sin 2\psi(B_2+B_3)] \tag{7b}$$

and

$$\dot{\psi} = \tfrac{1}{2}\gamma[-\tfrac{1}{2}\sin 2\phi\sin 2\psi\{B_1+\cos^2\theta(B_1+B_2+B_3)\} + \cos\theta\cos 2\phi\{B_1\cos 2\psi + B_2\cos^2\psi - B_3\sin^2\psi\}]. \tag{7c}$$

These equations describe the rotation of the particle subsequent to arbitrary initial conditions for θ, ϕ, ψ, where γ is either constant, or (as a consequence of the Stokes flow assumption) time-dependent. Hinch & Leal (1979) also give these equations, but in terms of differently defined Euler angles. In general, the motion is a complicated

† Gierszewski & Chaffey (1978) give these equations with wrong signs. The computations presented by them were, however, based on the correct form of the equations (private communication, 1978).

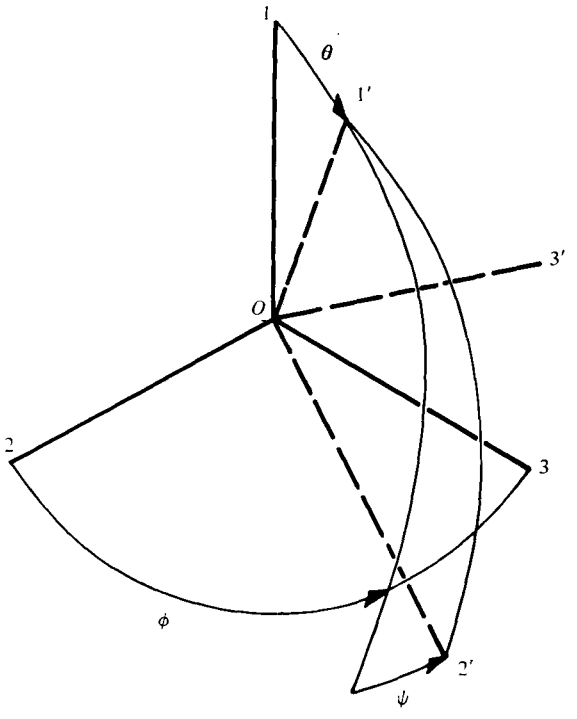

FIGURE 1. Euler angles. $O123$ fixed in space. $O1'2'3'$ fixed in particle.

tumbling. However, it is clear that there are three orbits in which the motion is simply periodic, and that the corresponding equations of motion involve only one of the B_i in each case. The cases are as follows:

$$(1) \quad \theta = 0^\circ \quad (\textit{see figure } 2)$$

For this case the particle spins about its own $O1'$ axis with angular velocity, from $(6a)$,

$$\omega_1 = \dot{\phi} + \dot{\psi}. \tag{8}$$

Substituting from $(7a, c)$ and simplifying,

$$\dot{\phi} + \dot{\psi} = \tfrac{1}{2}\gamma[1 + B_1 \cos(2\phi + 2\psi)], \tag{9}$$

whence, provided $|B_1| < 1$, as in (3),

$$\tan(\phi + \psi) = \left(\frac{1+B_1}{1-B_1}\right)^{\frac{1}{2}} \tan[\tfrac{1}{2}\gamma T_1 (1 - B_1^2)^{\frac{1}{2}}] \tag{10}$$

and

$$B_1 = |[1 - (4\pi/\gamma T_1)^2]^{\frac{1}{2}}| \tag{11}$$

where T_1 is the period of rotation.

$$(2) \quad \theta = 90^\circ, \quad \psi = 0^\circ \quad (\textit{see figure } 3)$$

Equation $(7a)$ reduces to

$$\dot{\phi} = \tfrac{1}{2}\gamma - \tfrac{1}{2}\gamma B_2 \cos 2\phi, \tag{12}$$

whence, provided $|B_2| < 1$,

$$\tan\phi = \left(\frac{1-B_2}{1+B_2}\right)^{\frac{1}{2}} \tan[\tfrac{1}{2}\gamma T_2 (1 - B_2^2)^{\frac{1}{2}}] \tag{13}$$

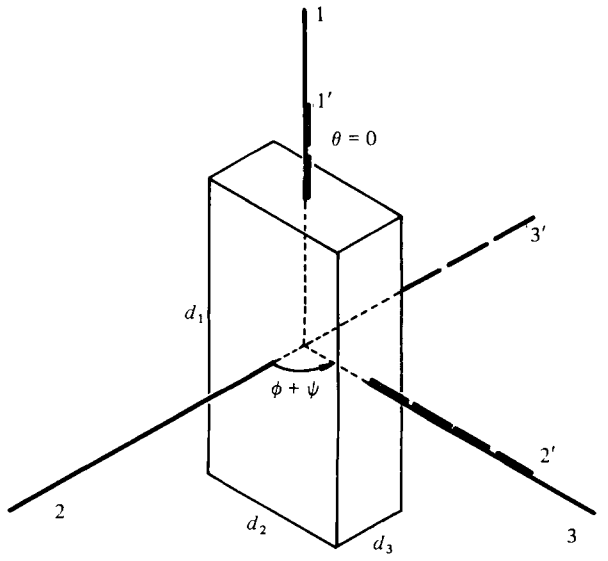

FIGURE 2. Periodic orbit case 1, shown at $\phi+\psi = 90°$.

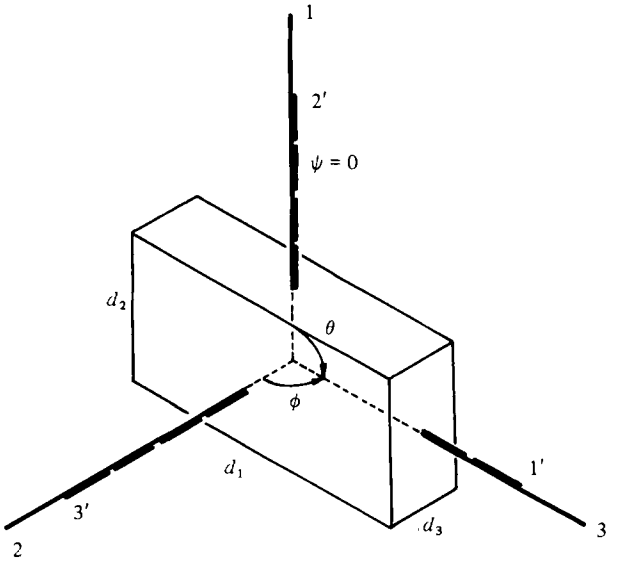

FIGURE 3. Periodic orbit case 2, shown at $\phi = 90°$.

and
$$B_2 = -|[1-(4\pi/\gamma T_2)^2]^{\frac{1}{2}}|. \tag{14}$$

(3) $\theta = 90°$, $\psi = 90°$ (*see figure* 4)

Equation 7 (a) reduces to
$$\dot{\phi} = \tfrac{1}{2}\gamma + \tfrac{1}{2}\gamma B_3 \cos 2\phi, \tag{15}$$
whence, provided $|B_3| < 1$,
$$\tan\phi = \left(\frac{1+B_3}{1-B_3}\right)^{\frac{1}{2}} \tan[\tfrac{1}{2}\gamma T_3(1-B_3^2)^{\frac{1}{2}}] \tag{16}$$

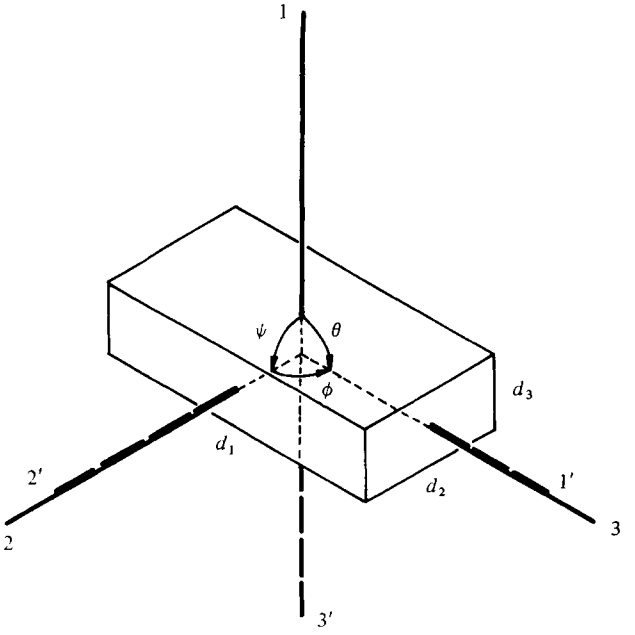

FIGURE 4. Periodic orbit case 3, shown at $\phi = 90°$.

and B_3 is given in terms of the period of rotation T_3 by

$$B_3 = |[1-(4\pi/\gamma T_3)^2]^{\frac{1}{2}}|. \tag{17}$$

The work by Hinch & Leal (1979) indicates that we may in some cases expect one or other of these orbits to be unstable, in the sense that if the particle is not initially aligned exactly as indicated, then it is capable of moving a substantial way from the desired position, rather than continuing to rotate close to it indefinitely. This would be most likely for long rods and platelets. However, we found that any drift away from the desired orbits was sufficiently slow for (11), (14) and (17) to be useful in obtaining values of B_i by timing the periods of rotation T_i.

3. Experimental procedure

The velocity field $v_3 = \gamma x_2$ was approximated in the annulus between Perspex cylinders counter-rotating about a vertical axis. The apparatus was that used previously by Harris & Pittman (1975). The annulus was 25 cm high, and bounded at radii of 12·6 and 15·3 cm. Continuously variable gears enabled one to vary independently the shear rate in the annulus and the position of the cylindrical fluid shell which is stationary relative to the observer. The suspending liquid was a Newtonian aqueous glucose solution with a viscosity at room temperature of approximately 7 poise. Particles were machined from Tufnol and measured with a micrometer. By judicious prodding they were set up in the special orbits mentioned above, and brought to rest (in the sense of translation) relative to the observer by making slight adjustments to the cylinder gearing. Half-periods of rotation were then timed. Observation was by eye. Each data point was obtained as the mean of four or five results.

The apparatus was kept covered as far as possible, to minimize water absorption from the air by the glucose solution, which was periodically mixed. Any bubbles thus introduced were allowed to clear before experiments were started and care was also taken to avoid bubbles adhering to the particles as they were introduced into the liquid.

To check on the values of B_i so obtained, particles were observed along the $O2$ axis (i.e. along a radius of the cylinders) executing general doubly periodic orbits. CCTV was used with a video-recorder, and the particle images filled most of a 16-inch monitor screen. To establish the horizontal $O3$ direction, the free surface of the liquid was filmed. To establish the magnification factor on the screen a particle was filmed stationary, with its longest side set up perpendicular to the viewing direction. Recordings of the particle motion were played back, and at any convenient instant the tape was stopped and the positions of the particle edges marked on the screen using a felt-tip pen. The tape was then wound on slowly, counting the frames (50 per second), stopped again after a suitable number and the new position marked. The procedure was continued as long as desirable, and finally the horizontal datum was marked.

A sheet of tracing paper was then taped onto the screen, the brightness turned full up, the markings traced and removed for analysis as follows. Let d_1, d_2, d_3 be the particle dimensions in the directions of the particle axes $O1'$, $O2'$, $O3'$, and $d_1 \geqslant d_2 \geqslant d_3$. The projections of d_1 and θ onto the $O13$ plane are measured. Call them l_1 and λ respectively. Then θ is given by

$$\sin\theta = \left|\left[1-\left(\frac{l_1}{d_1}\right)^2\cos^2\lambda\right]^{\frac{1}{2}}\right| \tag{18}$$

and ϕ from

$$\cos\phi = \left[1-\left(\frac{l_1}{d_1}\right)^2\right]^{\frac{1}{2}} \Big/ \left[1-\left(\frac{l_1}{d_1}\right)^2\cos^2\lambda\right]^{-\frac{1}{2}}. \tag{19}$$

In principle, ψ can be found by measuring α, the angle between $O3$ and the projection of d_2 onto the $O13$ plane. Then

$$\tan\psi = \frac{-\sin\theta - \tan\alpha\sin\phi\cos\theta}{\tan\alpha\cos\phi}. \tag{20}$$

Alternatively, using the angle between $O3$ and the projection of the shortest side d_3, on to $O13$ (call it β) we have

$$\cot\psi = \frac{\sin\theta + \tan\beta\sin\phi\cos\theta}{\cos\phi\tan\beta}. \tag{21}$$

In practice it was found difficult to get sufficiently accurate values of α or β, and ψ was not determined experimentally.

4. Results and discussion

We first mention a set of experiments to determine B_i for six particles having the same dimensions $d_2 = 1{\cdot}75$ mm, $d_3 = 1{\cdot}28$ mm but with d_1 ranging from 9·5 to 2·5 mm. Four determinations of T_1 [see (11)] were made for each particle and the means taken. A pooled estimate of variance gave 95 % confidence limits for the means of $\pm 5\,\%$, and the means were found not to differ significantly at the 95 % confidence level. Thus in these experiments B_1 is, within experimental accuracy, a function only of d_2/d_3.

Now although for ellipsoids the B_i are each functions of only one of the axis ratios, we would in general expect B_i to depend on all three particle dimensions. Our results raise the interesting possibility that for cuboids, dependence upon the third dimension is, at most, weak. This suggests representing data on the B_i in terms of equivalent ellipse axis ratios P_i by analogy with (3):

$$B_1 = \frac{P_1^2 - 1}{P_1^2 + 1}, \tag{22}$$

$$B_2 = -\frac{P_2^2 - 1}{P_2^2 - 1} \tag{23}$$

and

$$B_3 = \frac{P_3^2 - 1}{P_3^2 + 1} \tag{24}$$

and we may find that, approximately,

$$\left.\begin{aligned} P_1 &= P_1(R_1), \\ P_2 &= P_2(R_2) \\ \text{and} \quad P_3 &= P_3(R_3), \end{aligned}\right\} \tag{25}$$

where $$R_1 = \frac{d_2}{d_3}, \quad R_2 = \frac{d_1}{d_3} \quad \text{and} \quad R_3 = \frac{d_1}{d_2}.$$

We do not imply by this that a cuboid corresponds in its rotation to any ellipsoid: for this to be so, we should need

$$P_3 = P_2/P_1 \tag{26}$$

or equivalently

$$B_1 B_2 B_3 + B_1 + B_2 + B_3 = 0, \tag{27}$$

which, presumably, is not in general true. An advantage of representing results in terms of P_i is that these quantities increase continuously with the T_i and are therefore more directly related to the experimental measurements than are the B_i.

Values of T_i and hence P_i were obtained for 18 further particles having dimensions ranging from 0·26 to 16 mm and volumes from 2 to 72 mm^3. We suspect from our preliminary experiments that the P_i *vs.* R_i relationship may be almost the same for the cases $i = 1, 2, 3$. Plots of the data for the three cases are shown in figures 5–7. Now a cube shares with a sphere the property $B_1 = B_2 = B_3 = 0$, so we should constrain any lines fitted to the data to pass through $P_i = 1$ at $R_i = 1$. A least-squares fit of the pooled data for $i = 1, 2, 3$ gave

$$P_i = R_i^{0.823} \tag{28}$$

with a mean-squared deviation of 0·090. This line is shown on the three figures and very few points lie more than 10 % off it.

However, figures 5–7 give the impression that points P_1 more often lie below the line and P_3 values lie above it, while for P_2 the data is scattered evenly. This probably indicates a very weak dependence upon the third particle dimension. The form in which this enters the relationship is unknown, and so we arbitrarily introduce a parameter h_i associated with P_i, where

$$\left.\begin{aligned} h_1 &= d_1/(d_2 d_3)^{\frac{1}{2}} \quad (2{\cdot}5\text{–}9), \\ h_2 &= d_2/(d_1 d_3)^{\frac{1}{2}} \quad (0{\cdot}4\text{–}3{\cdot}8) \\ \text{and} \quad h_3 &= d_3/(d_1 d_2)^{\frac{1}{2}} \quad (0{\cdot}08\text{–}0{\cdot}5). \end{aligned}\right\} \tag{29}$$

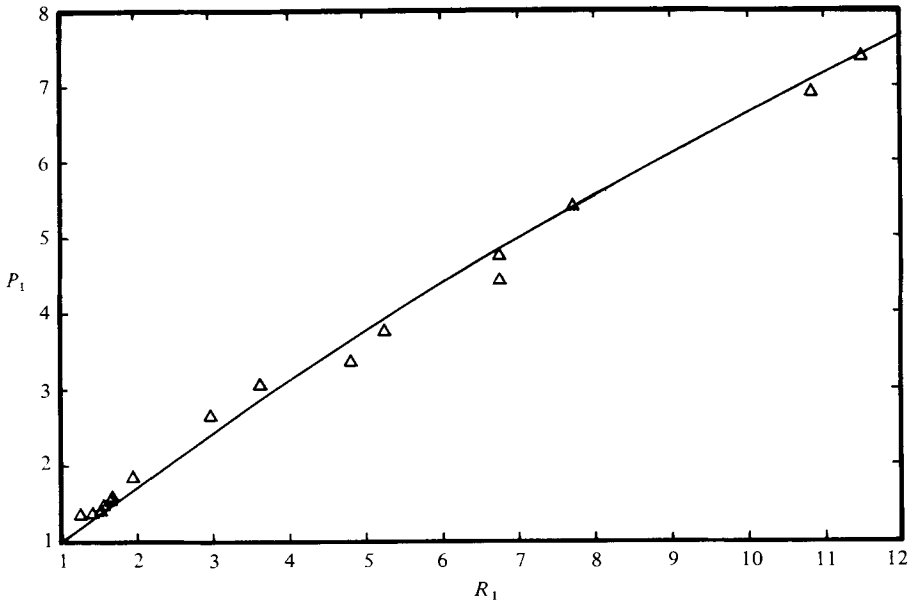

FIGURE 5. P_1 *vs.* R_1: △, experimental data points; ——, equation 28.

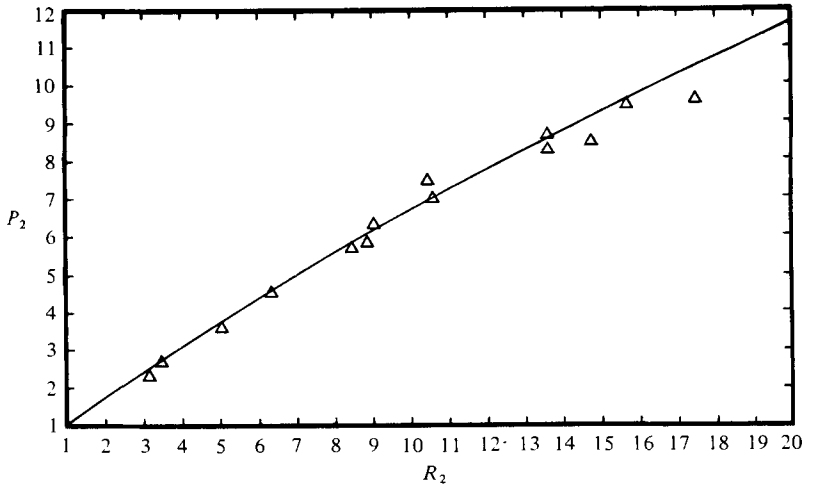

FIGURE 6. P_2 *vs.* R_2: △, experimental data points; ——, equation 28.

The bracketed figures indicate the range of values of h_i applying in our experiments. Presumably any dependence of P_i on h_i will be monotonic, and must be asymptotic to finite limits as h_i tends to zero or infinity. In view of the apparent smallness of the effect there is little justification for anything more elaborate than a single parameter function of h_i. We could also require the function to equal one when $h_i = 1$. Such a one is provided by $[\frac{1}{2}+(1+h_i)^{-1}]^C$ and we introduce it as a factor to the right-hand side of our fitted expression. Pooling the data for $i = 1, 2, 3$ we find

$$P_i = R_i^{0.825}\left(\frac{1}{2}+\frac{1}{1+h_i}\right)^{0.055}, \tag{30}$$

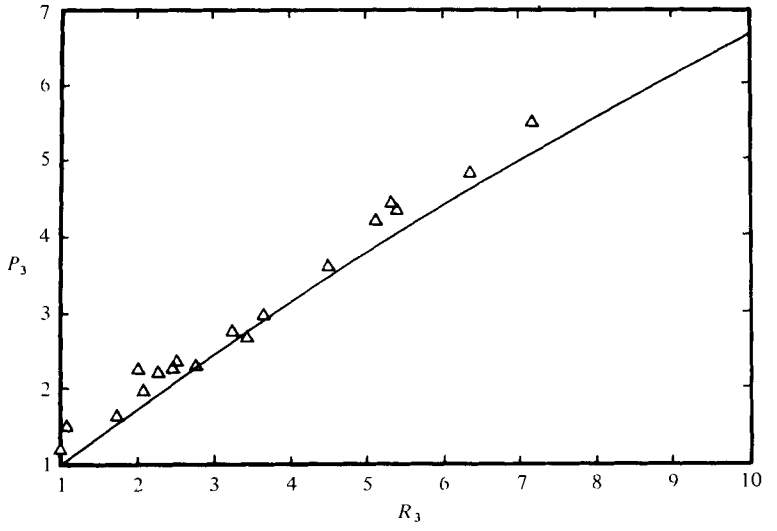

FIGURE 7. P_3 *vs.* R_3: △, experimental data points; ——, equation 28.

from which the data has a mean-squared deviation of 0·079. The positive value for C is consistent with our idea that the high values of h_1 are associated with P_1 values slightly below the mean line, etc. The mean squared deviation is also reduced very slightly. But the fitted expression indicates a dependence upon h_i of no more than a couple of per cent and most of the scatter in the data is apparently due to experimental errors. This is believed to arise very largely from small geometrical imperfections in the particles, and the difficulty of setting them up precisely in the required orbits.

The success of the B_i values, obtained from (30) and (22)–(24), in characterizing a general doubly-periodic motion is now examined. Consider an experiment carried out under the following conditions:

$$d_1 = 8{\cdot}05\,\text{mm}, \quad d_2 = 1{\cdot}78\,\text{mm}, \quad d_3 = 1{\cdot}24\,\text{mm},$$
$$R_1 = 1{\cdot}44, \quad R_2 = 6{\cdot}49, \quad R_3 = 4{\cdot}52,$$
$$h_1 = 5{\cdot}42, \quad h_2 = 0{\cdot}563, \quad h_3 = 0{\cdot}328.$$

From (31) $$P_1 = 1{\cdot}32, \quad P_2 = 4{\cdot}71, \quad P_3 = 3{\cdot}52.$$

Therefore from (22) to (25),

$$B_1 = 0{\cdot}268, \quad B_2 = -0{\cdot}914, \quad B_3 = 0{\cdot}851.$$

Initial conditions were taken from the video recording as

$$\lambda_0 = 0{\cdot}0°, \quad \alpha = -20°, \quad l_1 = 4{\cdot}15\,\text{mm},$$

giving $$\phi_0 = 0{\cdot}0°, \quad \theta_0 = 59{\cdot}0°, \quad \psi_0 = 67{\cdot}0°.$$

The shear rate $\gamma = -0{\cdot}97\,\text{s}^{-1}$.

Experimental measurements were made over 30 seconds, at intervals of 1 second. Theoretical results were obtained by a fourth-order Runge–Kutta integration of (7), incorporating the appropriate B_i, initial conditions and γ. Numerical results are correct to at least three significant figures. Comparisons for λ, θ, ϕ are shown in figures 8, 9 and 10.

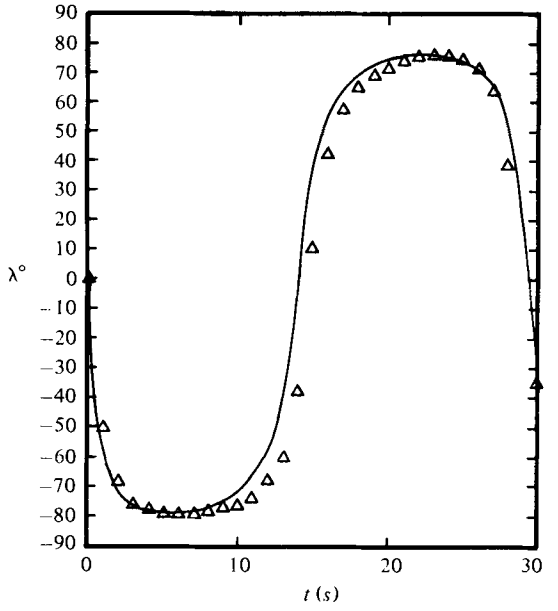

FIGURE 8. λ *vs.* t: $\triangle$, experiment aldata points; ——, computations. Doubly periodic orbit characterized by: $B_1 = 0{\cdot}268, B_2 = -0{\cdot}914, B_3 = 0{\cdot}851; \lambda_0 = 0°, \theta_0 = 59°, \phi_0 = 67°$.

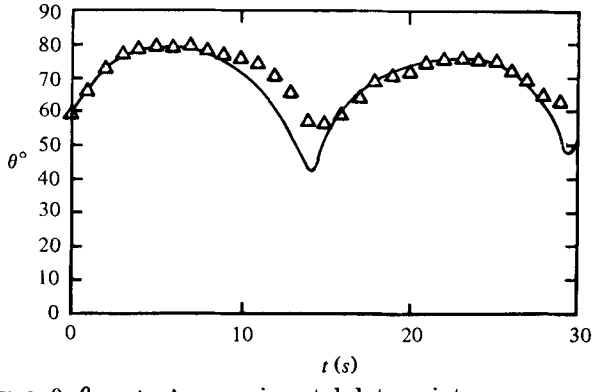

FIGURE 9. θ *vs.* t: $\triangle$, experimental data points; ——, computations. Orbit parameters as for figure 8.

Referring to figure 8 for λ, it is seen that the experimental maxima in $|\lambda|$ agree within about 1° with the computed maxima. The period of rotation (defined here as the time taken for λ to return to zero from positive values) shows agreement within a fraction of a second in about 30 seconds. Computed and experimental results, however, are out of step by something under 1 second at the mid-times. In figure 9 for θ, the maxima are once more given accurately, though the experimental results show a less sharp minimum than the computations, which are again about 1 second out of step at the mid-time. Figure 10 shows ϕ decreasing with time, since γ was negative in this experiment. A number of other runs gave similar relationships between experimental and computed orbits. Bearing in mind the difficulty, in this work, of making precise

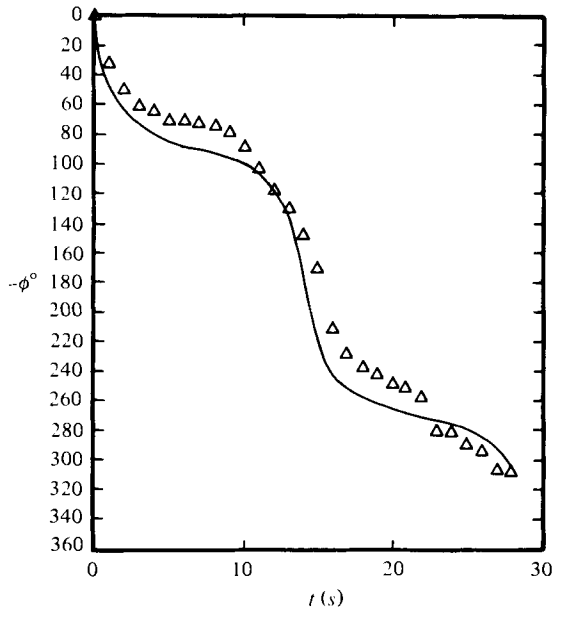

FIGURE 10. ϕ *vs.* t: △, experimental data points; ——, computations. Orbit parameters as for figure 8.

measurements, and the large number of parameters determining the particle motion (initial conditions for θ, ϕ, ψ together with B_i and γ) the agreement overall seems satisfactory. The difficulty in determining α accurately has already been mentioned and for this reason no results for ψ as a function of time are presented. However, a value of α had to be obtained to give the initial condition for ψ in the computation. This is a likely source of error, and numerical experiments showed how a change of a few degrees in the initial condition for ψ could have a significant effect on the computed orbit.

To illustrate the form of the motion over a longer period, we show in figures 11–13 results for computations in $0 \leqslant -\gamma t \leqslant 250$ (a negative γ was used in the experiments). In terms of a plot on the θ, ψ plane, as used by Hinch & Leal (1979), the present example is of an open orbit, rather than one which continuously loops round the points $\theta = \frac{1}{2}\pi$, $\psi = 0$ or $\frac{1}{2}\pi$. Further computations illustrated how very small changes in initial conditions or B_i values converted the orbit to this latter closed type, where θ passes through $\frac{1}{2}\pi$, a phenomenon never exhibited by bodies of revolution. The transformations under which equations (7) are invariant have been given by Gierszewski & Chaffey (1978), and have the same form as those given by Hinch & Leal (1979):

$$(\theta, \phi, \psi, t) \leftrightarrow (\theta, \phi + \pi, \psi, t) \tag{31a}$$

$$\leftrightarrow (\theta, \phi, \psi + \pi, t) \tag{31b}$$

$$\leftrightarrow (\pi - \theta, \phi, \pi - \psi, t) \tag{31c}$$

$$\leftrightarrow (\theta, \pi - \phi, \pi - \psi, -t). \tag{31d}$$

These show that the orbit is reflected about $\psi = n\pi$, $\pm n = 1, 2, 3, \ldots$ provided that at $\psi = n\pi$, $\phi = n\pi + \frac{1}{2}\pi$ radians. From figures 11 and 13 we see that at $\psi = 0°$, $\phi = -266°$, and when ψ first reaches $-180°$, $\phi = -108°$; the symmetries about $\psi = 0$ and $-180°$

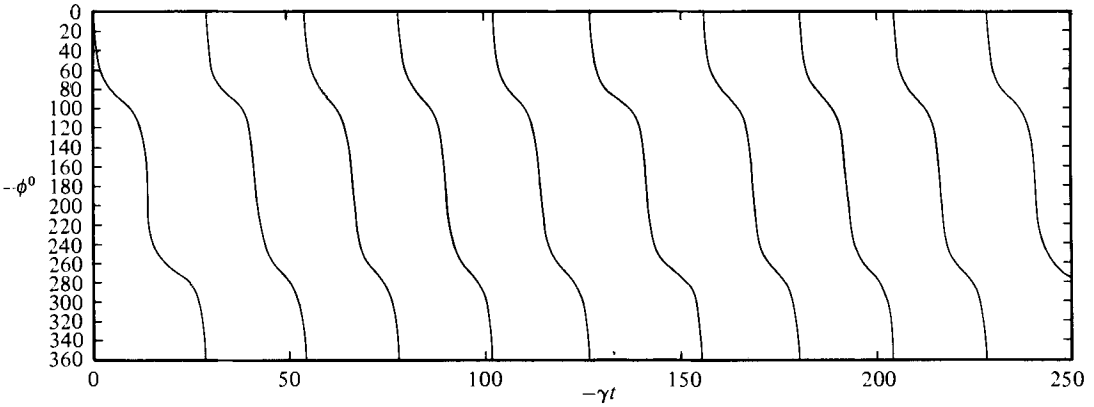

FIGURE 11. Computer predictions for ϕ. Orbit parameters as for figure 8.

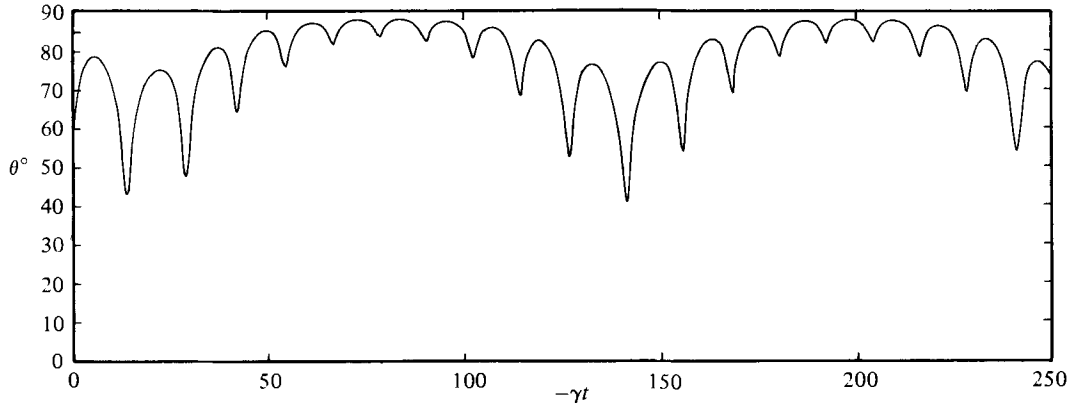

FIGURE 12. Computer predictions for θ. Orbit parameters as for figure 8.

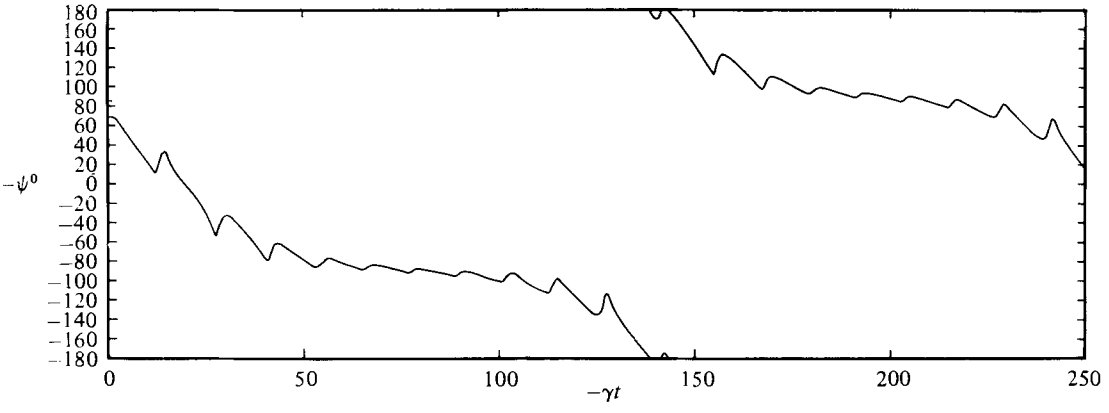

FIGURE 13. Computer predictions for ψ. Orbit parameters as for figure 8.

in figure 13 are thus only approximate. One similarly expects rough symmetry of ψ about $-90°$ and $-270°$, and of θ about its peak and minimum values. These features are evident in figures 12 and 13.

It now remains to decide how closely the experiments approached the idealization of a neutrally buoyant particle rotating without inertia effects in unbounded, plane Couette flow.

Settling rates for the particle were very low, being less than 0·01 cm s^{-1}. Moreover, in the special orbits used to determine B_i, forces due to vertical translation have no component in the direction of rotation and will not interact with it. In assessing inertia effects it is not clear how to choose the characteristic dimension of the particle. However, using the diameter of a sphere having the same volume as the largest particle used (72 mm^3), we get $d = 0{\cdot}5$ cm and the Reynolds number

$$Re = \gamma d^2/\mu = 0{\cdot}04.$$

The experiments of Poe & Acrivos (1975) for a sphere rotating in Couette flow show an increase of about 5 % in the period of rotation as the Reynolds number rises from zero to one. In similar experiments (Harris 1973), we have found that in the range $0 < Re < 1$ the period of rotation of a sphere T can be represented by $4\pi/(\gamma T) = 1 - 0{\cdot}039 Re^{\frac{3}{2}}$, which is consistent with this. In the absence of data on particles other than spheres, we take these results as indicating negligible inertia effects in the present work.

In discussing wall effects we use Brenner's (1962) result for an arbitrary particle rotating in a bounded Couette flow. The torque on the particle is related to that produced in an unbounded flow, L_∞, by

$$\frac{L}{L_\infty} = \frac{1}{1 - K(d/2l)^3 + \ldots},$$

where d is a characteristic particle dimension, l is a measure of its distance from the boundary (or boundaries) and K is determined by the form of the boundary. This result depends on certain assumptions which hold for the three orbits used to evaluate B_i, but do not hold for the general orbits. Available results indicate that taking $K = 1$ is likely to give a high estimate of wall effects in the present case. Given that the characteristic particle dimension occurs to the third power, its choice is crucial and can affect the predictions by one or two orders of magnitude. Taking $d = 0{\cdot}5$ cm, the largest equivalent sphere diameter, together with $2l = 2{\cdot}7$ cm, the annular gap width, one finds $L/L_\infty = 1{\cdot}007$. On the other hand, taking d equal to the largest dimension of any particle, 16 mm, an effect of 25 % is predicted, but this is surely unrealistic. An elongated particle will spend much of its time close to the streamlines, and the influence upon it of the cylinder walls will be very largely determined by its second and third largest dimensions. In no case was the second largest dimension of any particle greater than 0·3 cm. The analyses of Wakiya (1957) and Ho & Leal (1974) for spheres in bounded Couette flow also indicate negligible wall effects, based on $d = 0{\cdot}5$ cm.

Trevelyan & Mason (1951) concluded that flow field curvature in a concentric cylinder device of the type used here increased the effective shear rate by a fraction equal to $(d/R)^2$. In the experiments to determine B_i, d is now presumably taken as the largest horizontal dimension of the particle. R is the radius of curvature of the flow field. B_2 and B_3 will thus be more susceptible than B_1 to any effects which may occur. However taking the largest particle dimension, 16 mm, with the flow field radius of curvature, 14 cm, only 1·3 % change in the effective γ is predicted. Our results are believed to be accurate within ± 10 % in P_i.

The authors are grateful to Dr E. J. Hinch for showing them the paper by Hinch & Leal, prior to its publication, and for his helpful comments on an earlier draft of this paper.

REFERENCES

BRENNER, H. 1962 *J. Fluid Mech.* **12**, 35.
BRENNER, H. 1964 *Chem. Engng Sci.* **19**, 631.
BRETHERTON, F. P. 1962 *J. Fluid Mech.* **14**, 284.
GIERSZEWSKI, P. J. & CHAFFEY, C. E. 1978 *Can. J. Phys.* **56**, 6.
GOLDSMITH, H. L. & MASON, S. G. 1967 In *Rheology* (ed. F. R. Eirich), vol. 4, p. 89. Academic.
HARRIS, J. B. 1973 Internal Rep. Dept. Chem. Engng, University College, Swansea.
HARRIS, J. B. & PITTMAN, J. F. T. 1975 *J. Colloid Interface Sci.* **50**, 280.
HINCH, E. J. & LEAL, G. 1979 *J. Fluid Mech.* **92**, 591.
HO, P. B. & LEAL, L. G. 1974 *J. Fluid Mech.* **65**, 376.
JEFFERY, G. B. 1922 *Proc. Roy. Soc.* A **102**, 161.
POE, G. G. & ACRIVOS, A. 1975 *J. Fluid Mech.* **72**, 605.
TREVELYAN, B. J. & MASON, S. G. 1951 *J. Colloid Interface Sci.* **6**, 354.
WAKIYA, S. 1957 *J. Phys. Soc. Japan* **12**, 1130.
YOUNGREN, G. K. & ACRIVOS, A. 1975 *J. Fluid Mech.* **69**, 377.